CHEMPLUSCHEM

Supporting Information



# In Situ Methylation Transforms Aggregation-Caused Quenching into Aggregation-Induced Emission: Functional Porous Silsesquioxane-Based Composites with Enhanced Near-Infrared Emission

Yehao Yan, Richard M. Laine, and Hongzhi Liu*

## Reagents

Unless otherwise noted, all the reagents were purchased from commercial provider and used directly without further purification. Deionized water was used to replace tap water in the all experimental section. 1.2-dichloroethane was dried by $CaH_2$ and kept refluxing for 24 h.

## Theoretical calculation

The molecular LUMO and HOMO energy level were simulated by DFT Gaussian 09, and on the basis of B3LYP/6-31G (d). Besides, in the highest occupied molecular orbital (HOMO) level, electron donating group (M-TPA) possess higher electron cloud density, but electron withdrawing group DCM with higher electron cloud density in the lowest unoccupied molecular orbital level (LUMO), reveals the feature of ICT based on the push-pull process from M-TPA to DCM.

## Instruments

$^{1}H$ NMR and $^{13}C$ NMR spectra of the monomers were recorded by 500 MHz Bruker Avance, and dissolved in DMSO-$d_6$at room temperature with tetramethylsilane as the internal standard. The molecular weight of M-TPA-DCM was determined by Q-TOF6510 mass spectrometer (Agilent). The single-crystal of TPA-DCM and M-TPA-DCM with appropriate dimension waschosen under an optial microscope and quickly coated with high vacuum grease (Dow Corning Corporation). Intensity data and cell parameter were recorded by RigakuXtaLAB Synergy diffractometer coupled to a RigakuHypix detector with CuKα radiation (λ=1.54184Å) from PhotonJet micro-focus X-ray source. The spectra of UV-Vis were determined by Hitrachi spectrophotomer (UV-vis 4100). Fluorescence spectra were recorded through Hitrachi luminescence spectrophotometer F-7000 FL (Excitation wavelength: 485 nm, Speed: 2400 nm/min). Quartz cuvette, a container with 1-cm length and 3-cm height, was used in fluorescence and absorbance measurement. Silica gel ($60F_{254}$ Merck kGaA) was used to TLC.

Fourier-transform infrared (FTIR) spectra were recorded by Bruker Tensor 27 spectrophotometer with a disc of KBr from 4000 to 400 $cm^{-1}$ at a resolution of 4 $cm^{-1}$.

Solid-state $^{13}C$ cross polarization/magic angle spinning (CP/MAS) NMR and $^{29}Si$ MAS NMR spectra were memorized by Agilent DD2 700 NMR spectrometer. The crystallinity (PXRD) was measured with a Riguku D/MAX 2550 diffractometer with CuKα radiation, 40 kV, 200 mA with a 2θ range of 5-80 °(scanning speed of 10 °$min^{-1}$) at room temperature. The topography of composites were collected by High Resolution Transmission Electron Microscopy (HR-TEM, JEM 2100 electron microscope, JEOL, Japan) with acceleration voltage of 200 KV and Field Emission Scanning Electron Microscope (FE-SEM, HITACHI S4800). Thermogravimetric analyses (TGA) was measured by a Mettler-Toledo SDTA-854 TGA system in nitrogen (100 mL min-1) at a heating rate of 10 ℃ $min^{-1}$ from temperature to 750 ℃. Nitrogen adsorption-desorption isotherm measurements was conducted with QuadraSorb SI apparatus at 77 K. All samples were degassed at 150 ℃ for 12 h before measurement. Sample weight 100 mg and UHP-grade nitrogen (99.999%) gas source were employed in the nitrogen sorption measurements and collected by QuantachromeQuadrasorb apparatus. $S_{BET}$ was evaluated with $P/P_0$ in the range of 0.01 to 0.20. Nonlocal density functional theory (NL-DFT) pore-size distributions were confirmed by the carbon/slit-cylindrical pore mode of the Quadrawin software. Fluorescence quantum yield was recorded from FLS920 under the excitation of 445 nm laser and $BaSO_4$ as blank reference. Fluorescence lifetime was measured by a FLS920 with time correlated single photo counting (TCSPC) method with 445 nm excited laser. The data was deconvoluted with the instrument response function, recorded by reduced light, and fitted multi-exponential function.

## Preparation of metal ions and measurement of optical performance

The solutions multitudinous metal ions were prepared by corresponding metal salts dissolved into deionized water. $Cu^{2+}$, $Fe^{3+}$, $Ni^{2+}$, $Ru^{3+}$, $Co^{2+}$, $Zn^{2+}$, $Mg^{2+}$, $Cd^{2+}$, $Al^{3+}$, $Ag^{+}$, $Hg^{2+}$, $Mn^{2+}$ and $Pb^{2+}$ ($1.0\times10^{-2}$ mol/L) were prepared respectively by $Cu(NO_3)_2•3H_2O$, $FeCl_3•6H_2O$, $NiCl_2•6H_2O$, $RuCl_3$, $CoCl_2•6H_2O$, $Zn(NO_3)_2•6H_2O$, $MgSO_4$, $Cd(NO_3)_2•4H_2O$, $Al(NO_3)_3•9H_2O$, $AgNO_3$, $HgCl_2$ and $MnSO_4$. Typically, TPAIE-2 was applied to the exploration of fluorescence/absorbance performance. To

explore the selectivity of those materials, 3 mg of composite was added into the volume trick flask (10 mL) and distributed equably in mixed solution 10mL ($V_{Water}/V_{DMF}$=5:5, pH=7.0). Various metal ions were added into the above solutions respectively by micropipette and fluorescence measurement executed. To confirm the AIE effect, a series of untested solutions were prepared by change the fraction of water (from 0% - 90%) in testing system and recorded the variation of fluorescence. In addition, to conform the quantitative monitoring for $Ru^{3+}$, various volumes of $Ru^{3+}$ are added into the same solution and measure their fluorescence variation.

## Cultivation of single crystal

5 mg TPA-DCM and M-TPA-DCM have dissolved into dichloromethane 2 mL respectively, then, 6 mL ethyl acetate and 5 mL petroleum ether were added. Ultrasound for 10 minutes, place in 4 ℃ condition and maintain 20 days.

## Contents

**Table.S3** The composition, surface area and porosity data of TPAIEs.

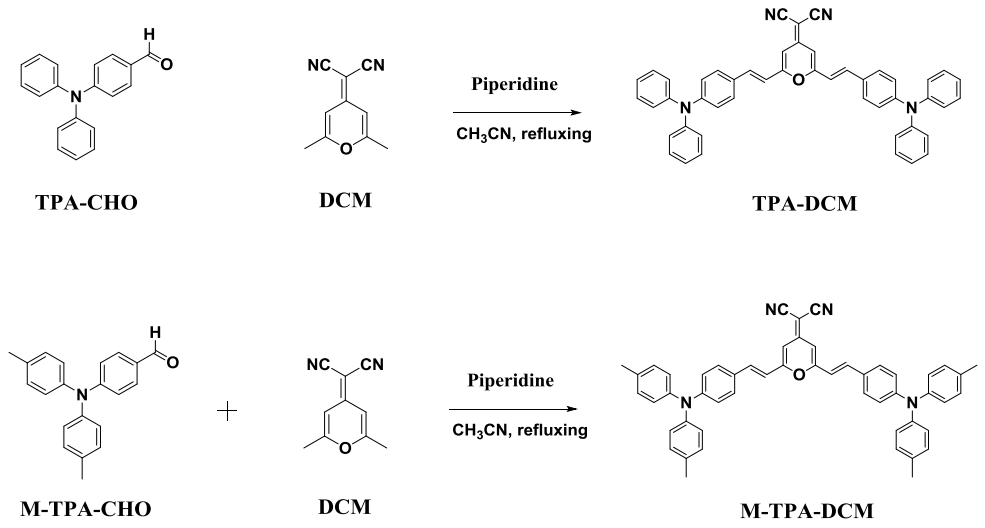


**Scheme S1** Synthesis route of TPA-DCM and M-TPA-DCM.

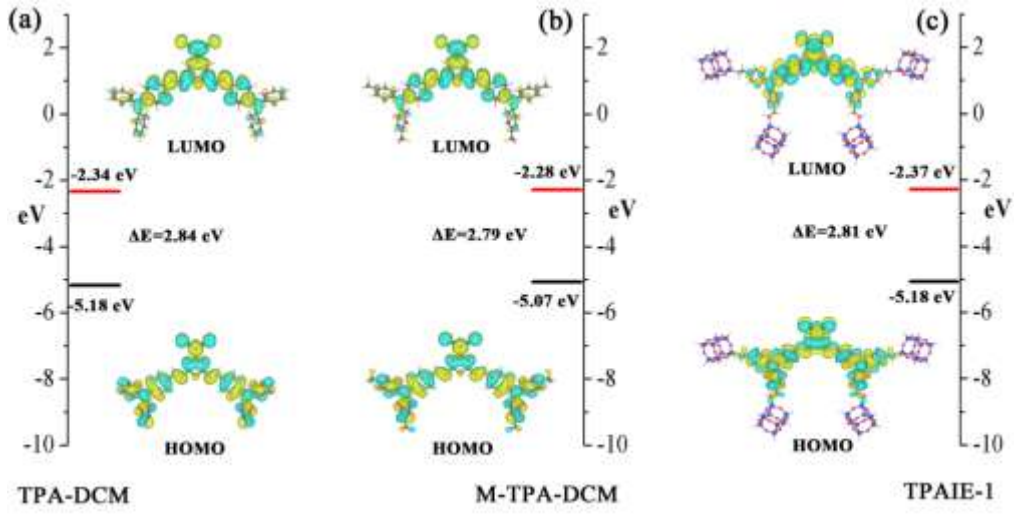


**Fig. S1(a)** Molecular orbital maps (HOMO and LUMO) of TPA-DCM; **(b)** Molecular orbital maps (HOMO and LUMO) of M-TPA-DCM; **(c)** Frontier molecular orbital map (HOMO and LUMO) simplified and optimized functional fragment of TPAIE-1.

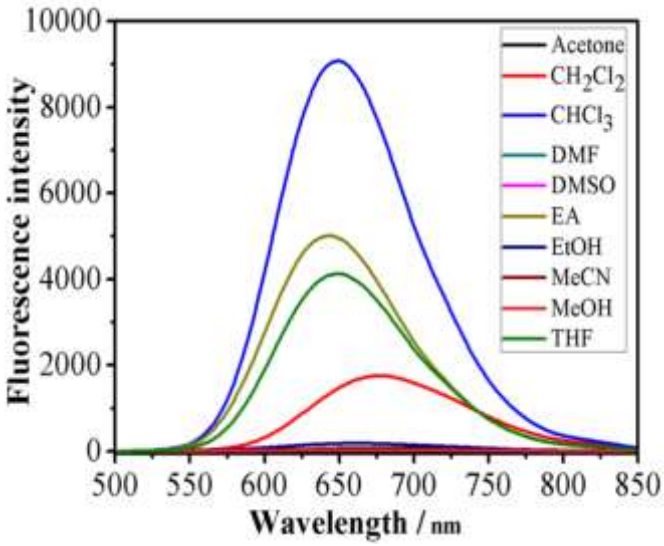


**Fig. S2** Solvent effect of M-TPA-DCM in various solvents with $10^{-4}$ M. (Excitation wavelength: 485 nm, Speed: 2400 nm/min, Slit: 5/5)

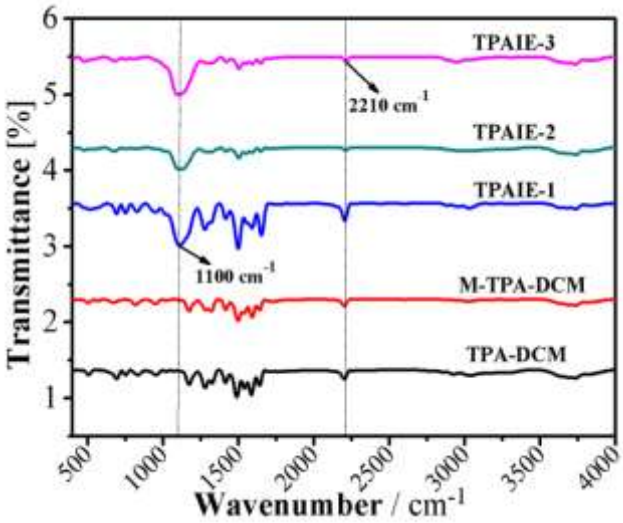


**Fig. S3** FT-IR spectra of TPA-DCM, M-TPA-DCM and TPAIEs.

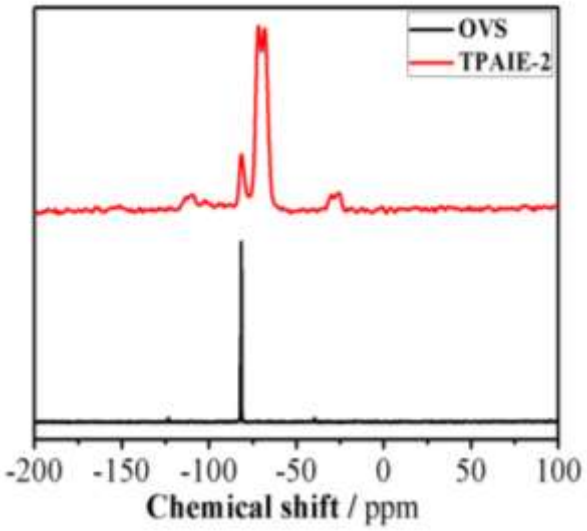


**Fig. S4** Solid state $^{29}$Si CP/MAS NMR spectra of OVS and TPAIE-2.

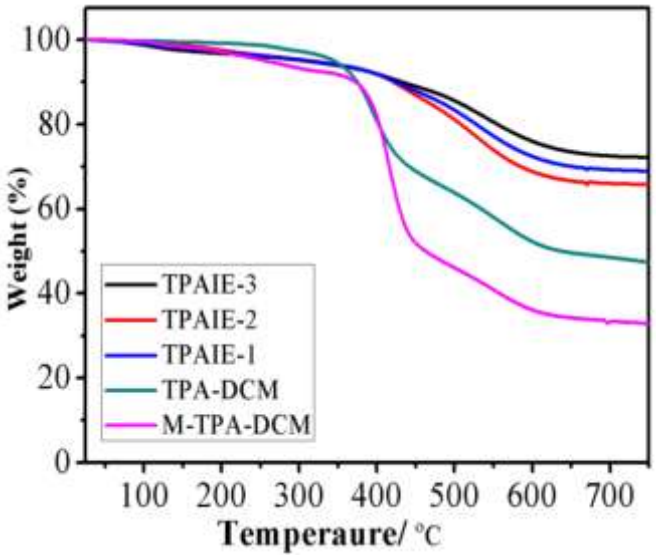


**Fig. S5** TGA curves of TPA-DCM, M-TPA-DCM and TPAIEs.

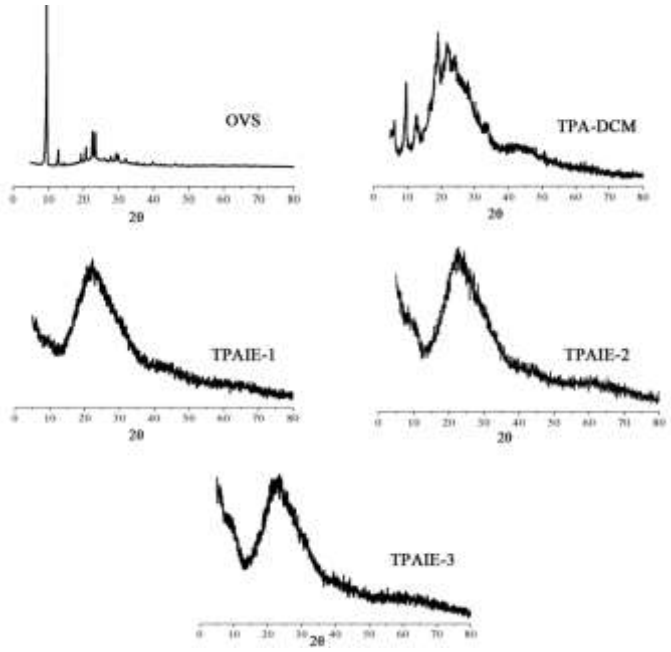


**Fig. S6** PXRD curves of OVS, TPA-DCM and TPAIEs.

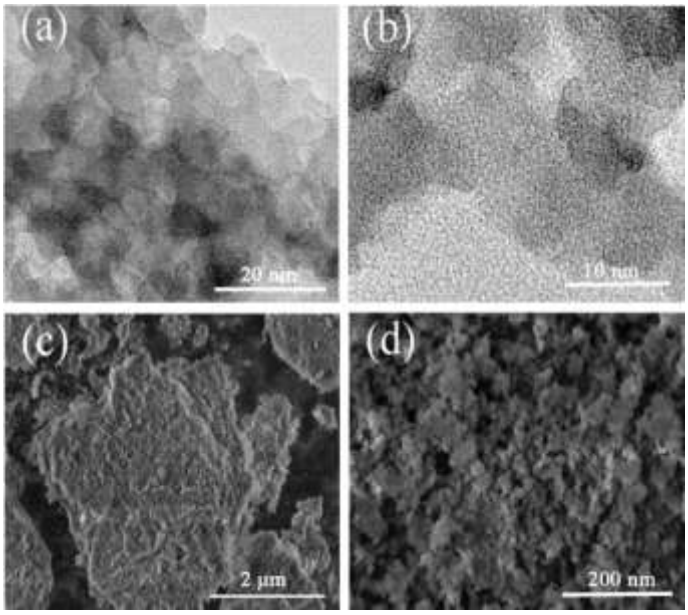


**Fig. S7** HR-TEM images of TPAIE-2 **(a)** and **(b);** FE-SEM images of TPAIE-2, **(c)** and **(d)**.

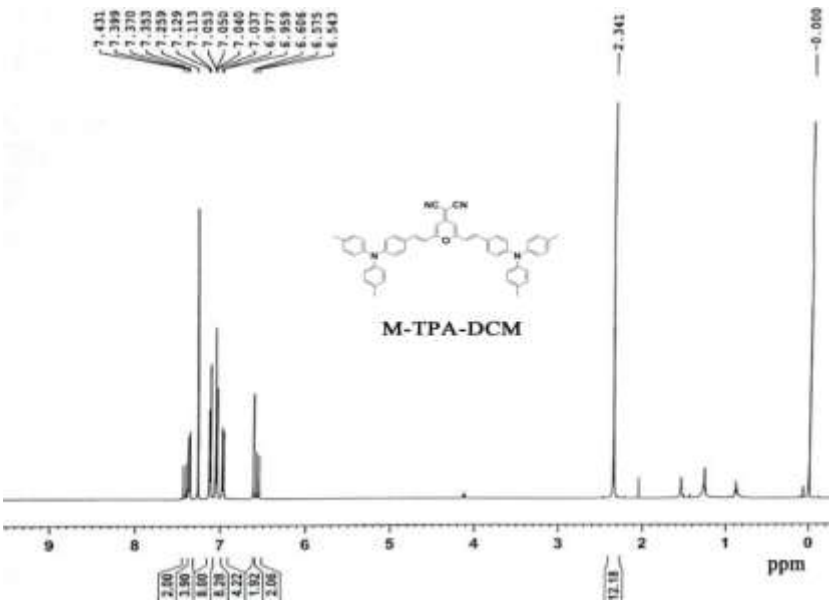


**Fig. S8** $^{1}$H NMR spectrum of M-TPA-DCM (500 MHz, $d_6$-DMSO).

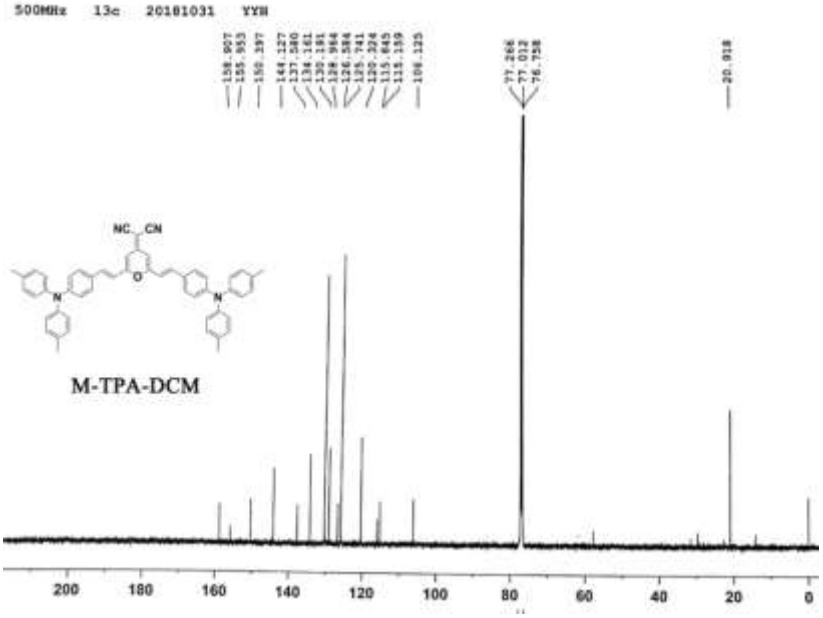


**Fig. S9** $^{13}$C NMR spectrum of M-TPA-DCM (125 MHz, $d_6$-DMSO).

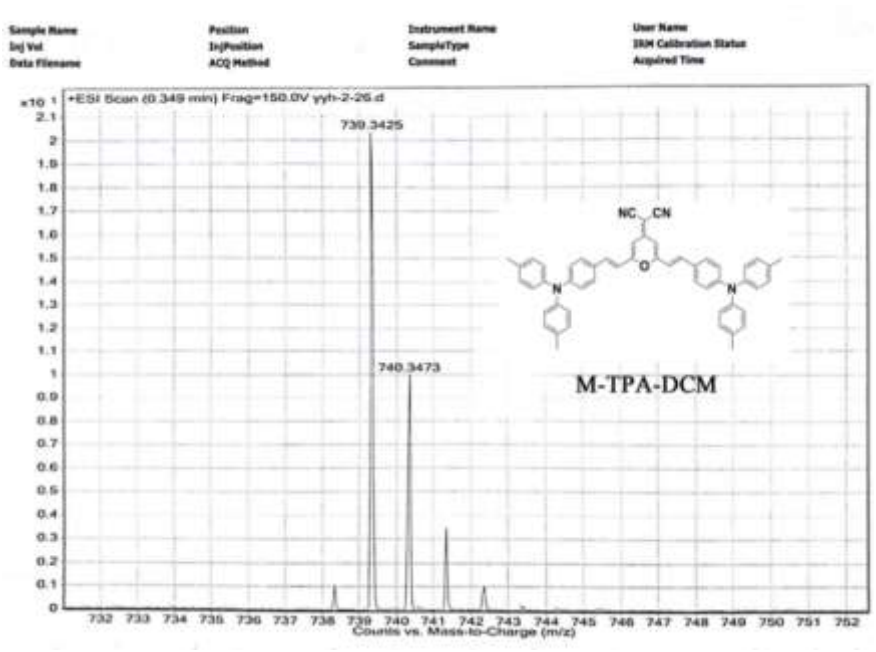


**Fig. S10** HR-MS spectrum of M-TPA-DCM.

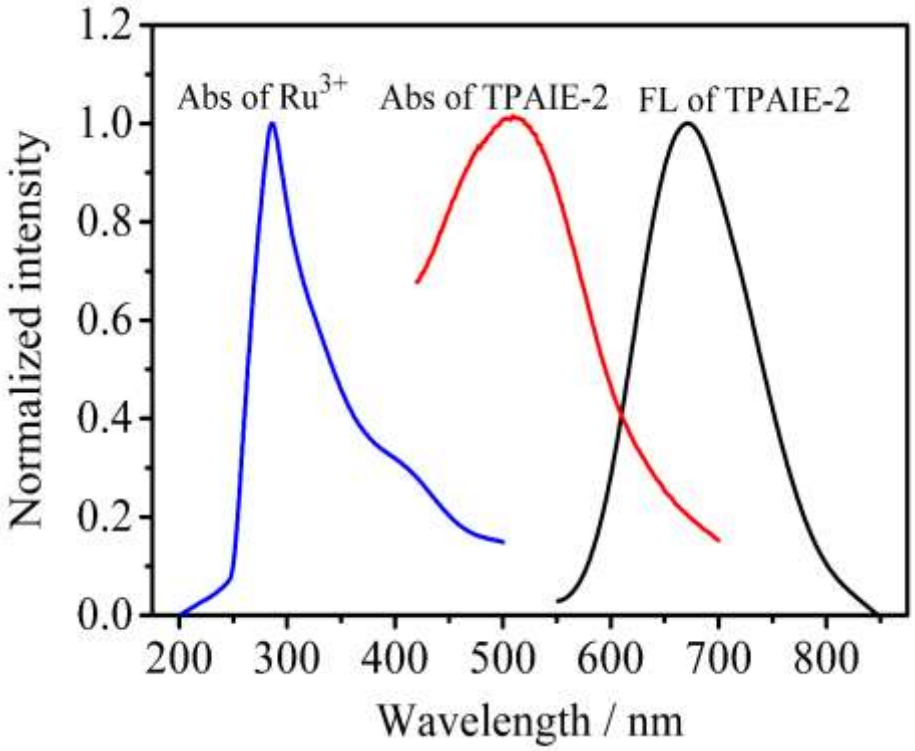


**Fig. S11**The fluorescence and absorbance spectra of $Ru^{3+}$and TPAIE-2.

**Table S1. Crystal data and structure refinement for TPA-DCM**

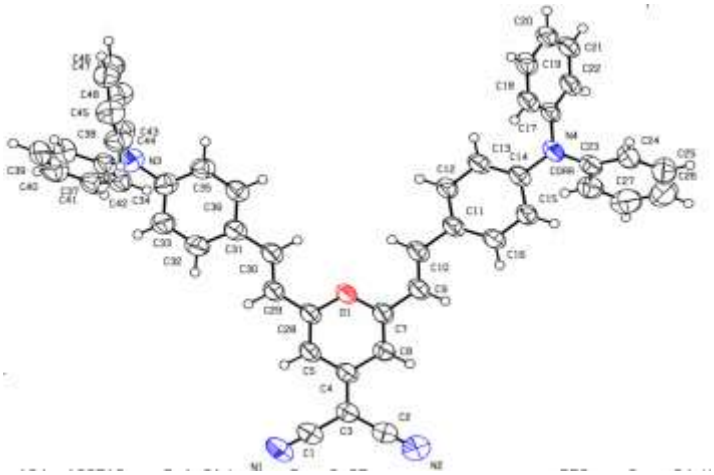

| **Table S1 Crystal data and structure refinement for TPA-DCM.** | |
|---|---|
| Identification code | 180716a_sq_s |
| Empirical formula | $C_{48}H_{34}N_4O$ |
| Formula weight | 682.79 |
| Temperature/K | 173(2) |
| Crystal system | monoclinic |
| Space group | $P2_1/n$ |
| a/Å | 19.8758(6) |
| b/Å | 7.4741(2) |
| c/Å | 28.9947(9) |
| α/° | 90 |
| β/° | 96.076(3) |
| γ/° | 90 |
| Volume/Å$^3$ | 4283.1(2) |
| Z | 4 |
| $\rho_{calc}$g/cm$^3$ | 1.059 |
| μ/mm$^{-1}$ | 0.498 |
| F(000) | 1432.0 |
| Crystal size/mm$^3$ | 0.05 × 0.02 × 0.01 |
| Radiation | CuKα (λ = 1.54184) |
| 2Θ range for data collection/ ° | 9.798 to 134.15 |
| Index ranges | -23 ≤ h ≤ 19, -8 ≤ k ≤ 8, -29 ≤ l ≤ 34 |
| Reflections collected | 24418 |
| Independent reflections | 7561 [$R_{int}$ = 0.0450, $R_{sigma}$ = 0.0386] |
| Data/restraints/parameters | 7561/0/478 |
| Goodness-of-fit on $F^2$ | 1.038 |
| Final R indexes [I>=2σ (I)] | $R_1$ = 0.0654, $wR_2$ = 0.1905 |
| Final R indexes [all data] | $R_1$ = 0.0912, $wR_2$ = 0.2139 |
| Largest diff. peak/hole / e Å$^{-3}$ | 0.23/-0.17 |

**Table S2. Crystal data and structure refinement for M-TPA-DCM**

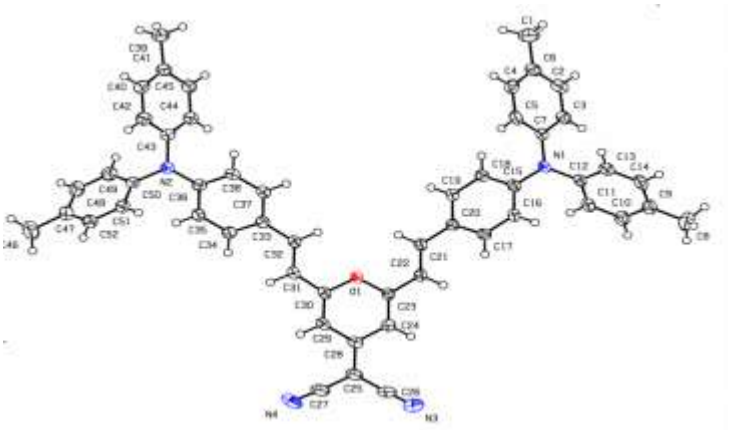

| **Table S2 Crystal data and structure refinement for M-TPA-DCM.** | |
|---|---|
| Identification code | 180917a_sq_s |
| Empirical formula | $C_{52}H_{42}N_4O$ |
| Formula weight | 738.89 |
| Temperature/K | 173(2) |
| Crystal system | monoclinic |
| Space group | $P2_1/n$ |
| a/Å | 19.7975(4) |
| b/Å | 10.1169(2) |
| c/Å | 23.8679(5) |
| α/° | 90 |
| β/° | 104.165(2) |
| γ/° | 90 |
| Volume/Å$^3$ | 4635.13(17) |
| Z | 4 |
| $\rho_{calc}$g/cm$^3$ | 1.059 |
| μ/mm$^{-1}$ | 0.492 |
| F(000) | 1560.0 |
| Crystal size/mm$^3$ | 0.05 × 0.03 × 0.02 |
| Radiation | CuKα (λ = 1.54184) |
| 2Θ range for data collection/° | 9.214 to 134.148 |
| Index ranges | -23 ≤ h ≤ 23, -12 ≤ k ≤ 4, -28 ≤ l ≤ 27 |
| Reflections collected | 25732 |
| Independent reflections | 8169 [$R_{int}$ = 0.0572, $R_{sigma}$ = 0.0586] |
| Data/restraints/parameters | 8169/0/518 |
| Goodness-of-fit on $F^2$ | 1.054 |
| Final R indexes [I>=2σ (I)] | $R_1$ = 0.0513, $wR_2$ = 0.1209 |
| Final R indexes [all data] | $R_1$ = 0.0731, $wR_2$ = 0.1339 |
| Largest diff. peak/hole / e Å$^{-3}$ | 0.21/-0.22 |

**Table S3** The composition, surface area and porosity data of TPAIEs.

**Table S3 Porosity of TPAIEs**

| Sample | Molar ratio of [OVS/TPA-DCM] | $S_{BET}$ [$m^2 g^{-1}$][a] | $S_{micro}$ [$m^2 g^{-1}$][b] | $V_{total}$ [$cm^3 g^{-1}$][c] | $V_{micro}$ [$cm^3 g^{-1}$][d] | $V_{micro}/V_{total}$ | Pore size [nm] |
|---|---|---|---|---|---|---|---|
| TPAIE-1 | 1:2 | 157 | 58 | 0.13 | 0.03 | 0.23 | 1.41 |
| TPAIE-2 | 3:2 | 718 | 323 | 0.55 | 0.16 | 0.29 | 1.54 |
| TPAIE-3 | 5:2 | 635 | 208 | 0.45 | 0.09 | 0.20 | 3.79 |

[a] Surface area calculated from the $N_2$ adsorption isotherms by the BET method. [b] Microporous surface area calculated from the $N_2$ adsorption isotherms by the t-plot method. [c] Total pore volume calculated at $P/P_0 = 0.99$. [d] Micropore volume derived by using the t-plot method rely on the Halsey thickness equation.

## Reference


[1] W. Qin, D. Ding, J. Liu, W. Z. Yuan, Y. Hu, B. Liu and B. Z. Tang, *Adv. Funct. Mater.* **2012**, *22*, 771-779.

[2] Y. Wu, D. Wang, L. Li, W. Yang, S. Feng and H. Liu, *J. Mater. Chem. A* **2014**, *2*, 2160-2167.